Chinese Chemical Letters 36 (2025) 110143

Contents lists available at ScienceDirect

Chinese Chemical Letters

journal homepage: www.elsevier.com/locate/cclet

UV-assisted ratiometric fluorescence sensor for one-pot visual detection of *Salmonella*

Ren Shen[a,c], Yanmei Fang[b], Chunxiao Yang[b], Quande Wei[b], Pui-In Mak[a,c], Rui P. Martins[a,c,d], Yanwei Jia[a,c,e,*]

[a] State-Key Laboratory of Analog and Mixed-Signal VLSI, Institute of Microelectronics, University of Macau, Macau, China
[b] Zhuhai Center for Disease Control and Prevention, Zhuhai 519000, China
[c] Faculty of Science and Technology – ECE, University of Macau, Macau, China
[d] On Leave from Instituto Superior Técnico, Universidade de Lisboa, Portugal
[e] MoE Frontiers Science Center for Precision Oncology, University of Macau, Macau, China

ARTICLE INFO

Article history:
Received 3 April 2024
Revised 7 June 2024
Accepted 19 June 2024
Available online 20 June 2024

Keywords:
Bacteria detection
Polymerase chain reaction
Naked-eye visualization
Ratiometric fluorescence
Smartphone app

ABSTRACT

Rapid diagnosis of *Salmonella* is crucial for the effective control of food safety incidents, especially in regions with poor hygiene conditions. Polymerase chain reaction (PCR), as a promising tool for *Salmonella* detection, is facing a lack of simple and fast sensing methods that are compatible with field applications in resource-limited areas. In this work, we developed a sensing approach to identify PCR-amplified *Salmonella* genomic DNA with the naked eye in a snapshot. Based on the ratiometric fluorescence signals from SYBR Green I and Hydroxyl naphthol blue, positive samples stood out from negative ones with a distinct color pattern under UV exposure. The proposed sensing scheme enabled highly specific identification of *Salmonella* with a detection limit at the single-copy level. Also, as a supplement to the intuitive naked-eye visualization results, numerical analysis of the colored images was available with a smartphone app to extract RGB values from colored images. This work provides a simple, rapid, and user-friendly solution for PCR identification, which promises great potential in molecular diagnosis of *Salmonella* and other pathogens in field.

Salmonella enterica, as one of the most prevalent pathogens in foodborne and waterborne diseases, is causing global health issues on a monthly basis [1–3]. It is especially life-threatening in resource-limited settings, where proper food handling and clean drinking water supply cannot be guaranteed [4–6]. Conventional diagnostics for *Salmonella* are culture-based methods coupled with serological tests, requiring days for results to come out [7,8]. These time-consuming and labor-intensive processes are undesired since fast identification of pathogens is a necessity for prompt disease control actions, especially in case of food safety incidents.

Detection of bacterial genetic materials using nucleic acid amplification test (NAAT) is an alternative and more advanced method for *Salmonella* diagnostics, with results coming out within hours [9–11]. Among the various NAAT approaches, Polymerase Chain Reaction (PCR) has been regarded as the gold standard for molecular diagnosis due to its high sensitivity and high specificity [12]. However, conventional PCR detection methods either require expensive fluorescence sensing apparatus [13] or trained operators to perform gel electrophoresis [14]. Both are not feasible in resource-limited settings when *Salmonella* outbreaks occur.

To promote on-site applications of PCR-based technologies, efforts have been made to achieve naked-eye visualization of PCR products. For example, Yamashige *et al.* [15] proposed a genetic alphabet expansion system for the visual detection of PCR amplicons. The scheme was successful with good sensitivity and specificity, but the requirement for three types of unnatural bases added to the expenses of this system and hindered its practicality in the field. Other approaches include exploiting nanoparticles, such as gold nanoparticles and copper nanoparticles, to make amplified nucleic acids naked-eye visible [16-20]. However, most nanoparticle-based visualization methods require additional steps to mix reagents and incubate the mixture upon completion of PCR. With an increased risk of cross-contamination, these post-amplification steps are to be avoided in all assays with DNA amplification involved.

Here, we established a one-pot naked-eye visualization approach to detect PCR products based on the ratiometric fluorescence from SYBR Green I (SG) and Hydroxyl naphthol blue (HNB).

* Corresponding author.
E-mail address: yanweijia@um.edu.mo (Y. Jia).

https://doi.org/10.1016/j.cclet.2024.110143
1001-8417/

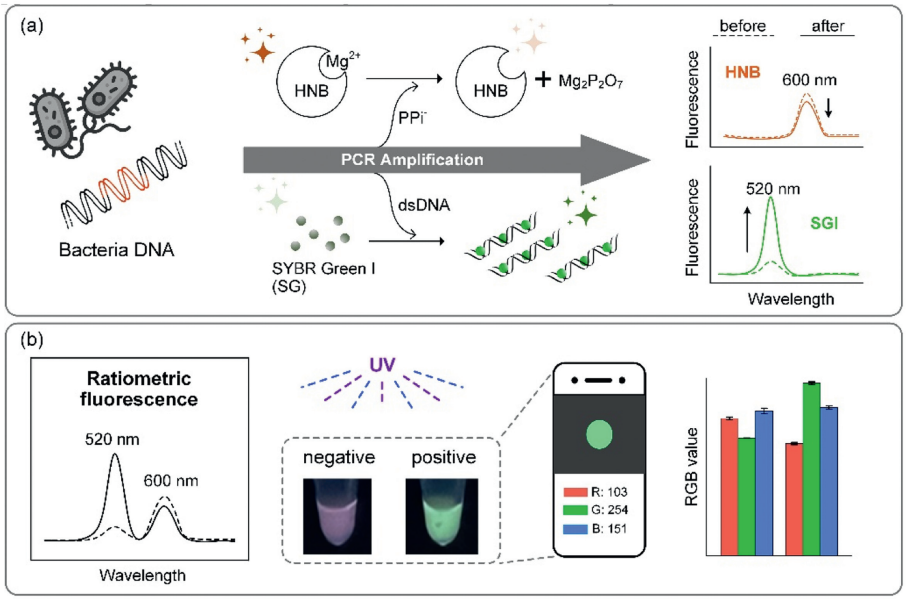

Fig. 1. Illustration of the visual detection scheme of *Salmonella* DNA based on ratiometric fluorescence signals. (a) The mechanism of ratiometric fluorescence signals from SG and HNB during PCR. (b) Naked-eye visualization of PCR products under UV excitation and RGB analysis of the images.

SG is a widely applied dsDNA-binding dye that emits an enhanced green fluorescence upon intercalation with double-stranded DNA [21,22]. HNB is a magnesium ion (Mg^{2+}) indicator that induces a weakened red fluorescence upon successful amplification [23,24]. Although neither SG nor HNB generates naked-eye observable fluorescence signals when they are used alone in PCR, the combinational use of the two dyes could result in a highly distinguishable colorimetric pattern under excitation of ultraviolet (UV) light, as Fig. 1 illustrates. With a thorough exploration of this sensing scheme, we applied it for one-pot detection of PCR targeting the specific genetic materials of *Salmonella* and achieved single-copy sensitivity and satisfactory specificity. Further, with a ready-to-use smartphone app, simple RGB analysis provided numerical indicators of the colored images. Apart from detecting *Salmonella*, the proposed PCR sensing scheme also opens up the possibility of on-site applications targeting a broad range of pathogens. The simplicity and cost-effectiveness of this approach would further promote PCR-based applications in point-of-care settings and resource-limited regions.

The reagents and materials used in this work were as follows. The stock of SG was 10,000× in dimethyl sulfoxide and was obtained from Invitrogen, USA. The working solution of SG was diluted to be 10× in deionized water (Millipore, USA) and stored in aliquots at −20 °C. HNB was obtained from Sigma-Aldrich, USA, and the stock powder was dissolved in deionized water (Millipore, USA) to form a 3 mmol/L working solution, which was stored at 4 °C. 5× HF PCR buffer (including 7.5 mmol/L $MgCl_2$), iProof DNA polymerase, and dNTP mix (10 mmol/L each) were purchased from Bio-Rad, USA. PCR primers for *Salmonella* detection followed a reported work (forward primer: 5′-GTTGAGGATGTTATTCGCAAAGG-3′ [25]; reverse primer: 5′-GGAGGCTTCCGGGTCAAG-3′) and were synthesized by Sangon Biotech, China.

All bacterial strains were obtained from the Zhuhai Center for Disease Control and Prevention: *Salmonella enterica* (ATCC 14,028), Escherichia coli (*E. coli*, CICC 10421), *Enterococcus faecalis* (*E. faecalis*, ATCC 29212). The bacterial strains were grown on solid mediums and incubated at 37 °C for 18 h. The pure cultures were then collected using dispensable inoculation loops and suspended in 3 mL of normal saline. The turbidity of bacteria-containing solutions was tested using a Densimat Densitometer (Biomérieux, France) and adjusted to about 0.5 McF, with the bacteria concentration at about 7×10^7 CFU/mL. Bacteria genomic DNA was then extracted from the solution using a QIAamp DNA Mini kit (Qiagen, Germany). The extracted DNA was eluted into a 100 μL volume and quantified using a Qubit 3 Fluorometer (Invitrogen, USA).

The PCR reaction mixture consisted of 1× PCR buffer (including 1.5 mmol/L $MgCl_2$), 200 nmol/L of each dNTP, 0.2 units of iProof DNA polymerase, and 200 nmol/L of each primer. SG and HNB concentrations varied upon experiment design. Extracted bacteria genomic DNA was used as the template at a concentration of 3×10^5 copies per reaction unless otherwise stated. PCR assays were performed on a Bio-Rad CFX96 PCR cycler (Biorad, USA) with a thermal profile as follows: 98 °C for 30 s, then 50 cycles of 98 °C for 5 s plus 67 °C for 10 s. The PCR outcomes were either monitored in real-time under the SYBR channel of the PCR cycler or visualized *via* the naked eye with a setting described below.

After PCR completed, the endpoint products were excited by UV (365 nm) with a UV transilluminator (Major Science, USA). The colored images under UV excitation were photographed *via* the camera of a smartphone (iPhone 13Pro). For numerical analysis of visualization results, the colored images were analyzed using a free smartphone app (Color Collect from WXColor Tech Ltd., China) for extraction of RGB values.

Also, an emission spectra analysis was performed at room temperature using a SpectralMax M2e microplate reader (Molecular Devices, USA). The excitation was set at 365 nm and the emission intensity from 500 nm to 650 nm was recorded with a 10 nm increment. Deionized water (Millipore, USA) was used as the plate blank for background subtraction.

As the most widely used dsDNA-binding dye, SG emits a strong green fluorescence upon its intercalation into dsDNA domains and has been extensively applied as a nucleic acid amplification indicator. However, a key limitation in SG-based applications is the dye's inhibitory effect on amplification when it is used at a high concentration [26-29]. As Fig. S1 (Supporting information) reveals, 2× SG blocked PCR completely. In this context, the dye is commonly used at a concentration from 0.2× to 0.4× [27,29], which limits the observable fluorescence signal and makes naked-eye detection impossible. As Fig. 2a shows, at both 0.4× and 2× SG concentrations, positive samples could not be distinguished from the no-template-

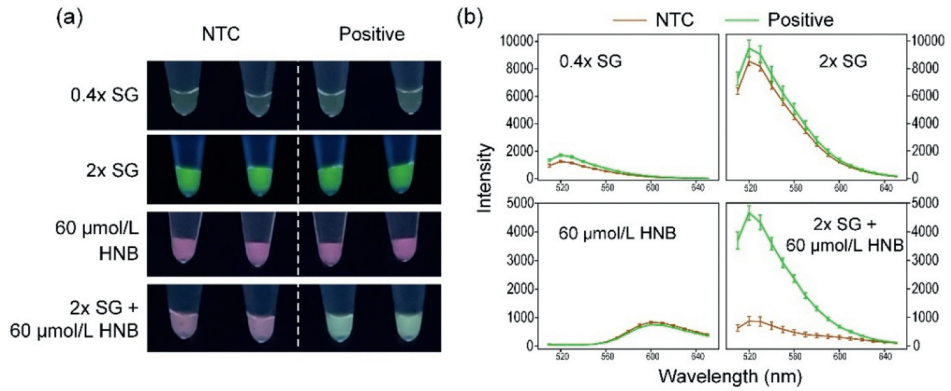

Fig. 2. Visualization of endpoint PCR results with different dye conditions (a) and corresponding emission spectra with excitation at 365 nm (b).

controls (NTC). At 0.4× SG, although possible samples emitted a slightly stronger fluorescence than the NTC, as quantitatively revealed in the emission spectra in Fig. 2b, the difference was too subtle to be seen *via* the naked eye. At 2× SG, the similarity in fluorescence intensity between NTC and "positive samples" that contained template DNA was due to amplification failures, as demonstrated in Fig. S1.

HNB represents another category of DNA amplification indicators, which function by monitoring ion levels during the amplification process. As a Mg^{2+} indicator, HNB competes with inorganic pyrophosphate (PPi), an amplification byproduct, to bind with magnesium ions [23,30]. Due to a reduced amount of HNB-Mg complex after amplification, a purple-to-blue color shift under natural light and a weakened red fluorescence are frequently reported in isothermal amplifications [31-34]. However, regardless of HNB's performance in isothermal amplifications, in PCR HNB could hardly generate any naked-eye distinguishable fluorescence or colorimetric signals (Fig. 2a and Fig. S2 in Supporting information). To the best of our knowledge, HNB's failure in reporting PCR outcomes might be due to a lower level of PPi generation in PCR as compared with that in isothermal amplification assays.

In this work, we found that SG's inhibitory effect on amplification could be offset by the inclusion of HNB in the reaction mixture (with details discussed in the next section). Thus, in the presence of HNB, a large amount of the SG dyes could be used without blocking PCR, raising SG's fluorescence to a great extent. As a result of the significantly enhanced green fluorescence from SG (emission peak at 520 nm) and the nearly constant red fluorescence from HNB (emission peak at 600 nm), the positive and negative amplification products displayed a high-contrast color difference under UV excitation. Direct visualization of endpoint PCR outcomes *via* the naked eye was made possible without any post-processing procedures. This provides a cost-effective and time-saving solution for detection of pathogenic bacteria such as *Salmonella*, as shown in Table S1 (Supporting information).

Compared with HNB's applications in isothermal amplification assays in reported work [24,31,35], HNB in this work was used at a relatively low concentration. Yet the low level of HNB has two important effects on the overall performance. Firstly, it canceled SG's inhibition of amplification and thus enabled the usage of SG at a high concentration. SG's inhibitory effect has been linked with its inhibition of the DNA polymerase and its high DNA affinity [26,27]. According to the work by Kong *et al.*, HNB could sequester dsDNA intercalating dyes such as EvaGreen in loop-mediated isothermal amplification (LAMP) and thus reduce the dye's inhibitory effect on the LAMP reaction [28]. This might also explain HNB's role in reducing SG's inhibition of PCR, as found in this work. As Figs. 3a and b reveal, when coupling 60 μmol/L HNB SG from 2× to up to 8× could be used in PCR with naked-eye distinguishable colorimetric patterns and without causing any delay in the C_q value in real-time PCR assays. As SG concentration increased, the green color became more obvious while the red color became less obvious. All four groups displayed high-contrast color patterns between NTC and positive samples, indicating a broad dynamic range.

8× SG does not define the upper limit of SG concentration, since more than 60 μmol/L HNB could be used to cancel the inhibitory effect as SG further increases. As Fig. S3 (Supporting information) shows, at 10× SG, increasing HNB concentration to 120 μmol/L or higher not only helped restore the PCR amplification process but also enabled naked-eye observable color change of endpoint products. Even a higher level of SG is possible with an accordingly increased concentration of HNB. The underlying mechanism of SG's inhibitory effect remains unclear and was linked with SG-polymerase interaction and SG degradation in some published work [22,36]. Since HNB participates in the amplification process mainly through its interaction with magnesium ions, our discovery that HNB could cancel SG's inhibitory effect might offer further insight into the interactions among DNA templates, SG, Mg, and the DNA polymerase.

Secondly, when HNB and SG were used in combination, the ratiometric fluorescence signals from SG and HNB rendered negative PCR samples and positive ones with high-contrast color patterns under UV excitation. Although HNB had a greatly weakened fluorescence as compared with SG (Fig. 2b), it provided a strong red color background under UV excitation. By tuning HNB concentration, various patterns of color transition could be achieved. As Fig. 3c displays, increasing HNB concentration resulted in changes as opposed to increasing SG concentration: red became more obvious while green turned less obvious. At 2× SG, a red-to-green color contrast could be observed between NTC and positive samples with a moderate HNB level (60–90 μmol/L), while pale-to-green at a low HNB level (30 μmol/L) and red-to-pale at a high HNB level (120 μmol/L or more).

To achieve highly distinguishable colorimetric patterns for naked-eye detection of PCR outcomes, using SG and HNB at proper concentrations is required. We thus screened various dye combinations to provide intuitive guidance on dye usage. As shown in Fig. 3d, the red dots represent reactions in which the red color dominated in both NTC and positive amplification products, indicating a superfluous HNB level or an insufficient SG concentration. The green dots represent reactions in which the green color dominated in both NTC and positive amplification products, mostly due to blocked amplification as a result of excessive SG and inadequate HNB. The black dots represent amplification reactions that displayed high-contrast colorimetric patterns in the endpoint outcomes. Based on these experiments, we roughly designated an ef-

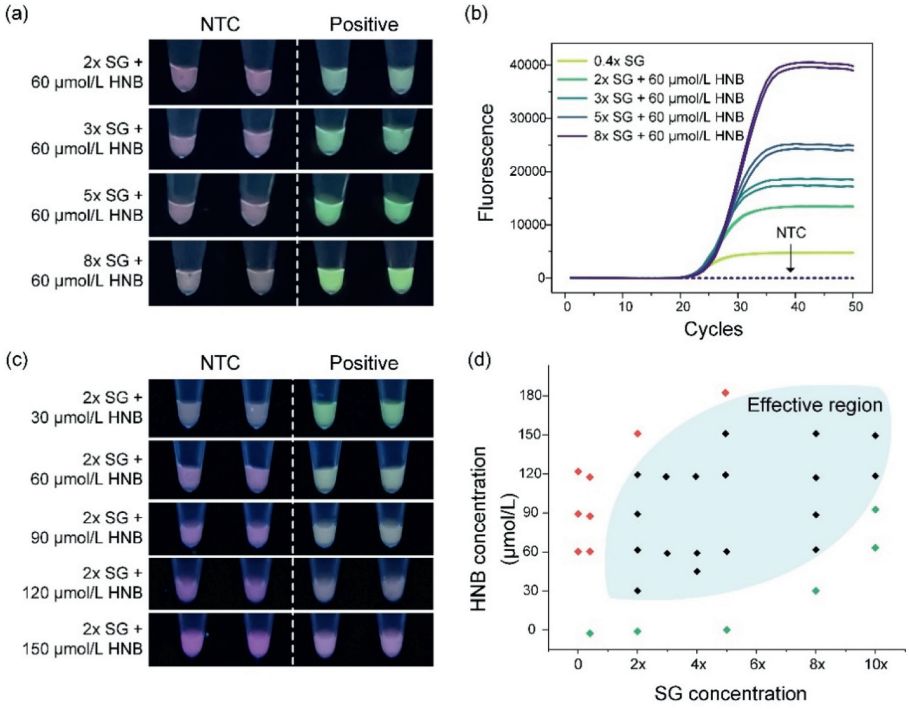

Fig. 3. Performance of the sensing system at various SG and HNB concentrations. (a) Naked-eye detection of PCR products with 60 μmol/L HNB and SG from 2× to 8×. (b) Real-time PCR amplification curves with 60 μmol/L HNB and SG from 2× to 8×. (c) Naked-eye detection of PCR products with 2× SG and HNB from 30 μmol/L to 150 μmol/L. (d) Visualization efficacy at various SG and HNB combinations. Red plots: both NTC and positive samples were red under UV excitation; Green plots: both NTC and positive samples were green; Black plots: a red/green contrast between NTC and positive samples. The blue area represents an effective region of dye combinations, within which naked-eye detection is achievable.

fective region (the blue area in Fig. 3d), within which dye combinations would bring about naked-eye visible PCR products. If a dye combination falls above the effective region, decreasing the HNB/SG ratio is suggested; on the other hand, if a dye combination falls under the effective region, the HNB/SG ratio should be increased to avoid inhibition of amplification and to achieve naked-eye visible results. As a preliminary instruction, the blue area in Fig. 3d does not indicate all possible effective dye combinations. As discussed above, further increasing SG concentration to over 10× and raising the HNB level correspondingly might also be applicable. Without any doubt, the wide dynamic range of dye combinations has demonstrated the robustness of our proposed sensing scheme.

For result consistency, the below experiments all used the combination of 2× SG and 60 μmol/L HNB unless otherwise stated. To validate the detection specificity of the established sensing approach, we examined the visualization results with various samples. Besides NTC and *Salmonella* gDNA, the genetic materials from *E. coli* and *E. faecalis* were also tested with PCR and visualized *via* the naked eye. As shown in Fig. 4a, the visualization results fell into three groups, with NTC samples being red, nonspecific samples being lavender, and the specific *Salmonella* samples showing a green color. Worth noticing is that the nonspecific samples displayed a color pattern different from the NTC samples, even though both *E. coli* and *E. faecalis* gDNA were not amplified through PCR, as revealed in Fig. 4b.

To explore in detail the color difference among various types of samples, we utilized a ready-to-use and free color-picking smartphone app [37] to extract the average Red, Green and Blue (RGB) values in a user-defined region of interest in the colored images and performed a simple RGB analysis. As Fig. 4c shows, compared with NTC, the specific *Salmonella* samples showed an enhancement in the green channel while the red and blue channels remained unchanged. This could be easily explained by the enhanced green fluorescence from SG due to the generation of a large amount of double-stranded amplicons. On the other hand, the nonspecific samples showed an obvious decrease in the red channel while no special change in the green and blue channels. Since there was no amplification with the nonspecific template DNA, the HNB fluorescence was unchanged and could not be the reason for the weakened red color. We attribute the reduced red value in nonspecific samples to a slightly increased SG fluorescence. Although *E. coli* and *E. faecalis* gDNA were not amplified through PCR, the double-stranded templates would increase SG fluorescence to a certain extent.

Although the PCR products can be directly viewed *via* the naked eye, a smartphone camera is often required to keep track of the visualization results, especially in field applications. To explore the influence of different smartphone configurations on the visual results, we used an iPhone 13Pro and a Redmi K60 to take photos of the endpoint PCR products (with 5× SG and 60 μmol/L HNB) for comparison. As shown in Fig. S4 (Supporting information), images were influenced by factors such as light exposure and white balance in the two smartphone cameras. However, the positive samples remained highly distinguishable from the negative samples in both images. Also, despite different RGB patterns in the two images, their Green/Red (G/R) ratios were roughly the same. In other words, different configurations of smartphone cameras do not affect the detection results. As a supplement to the intuitive naked-eye visualization results, the G/R ratio could serve as a good indicator to numerically analyze the color of endpoint amplification products. As shown in Fig. 4d, the G/R ratio of NTC samples was about 0.8, with that of specific *Salmonella* samples reaching 1.2 and that of nonspecific samples close to 1.0.

With the detection specificity already validated, we next sought to explore the detection limit of PCR-amplified *Salmonella* DNA with the ratiometric fluorescence sensing scheme. As shown in Fig. 5a, after 50 cycles, samples displayed a green color with as

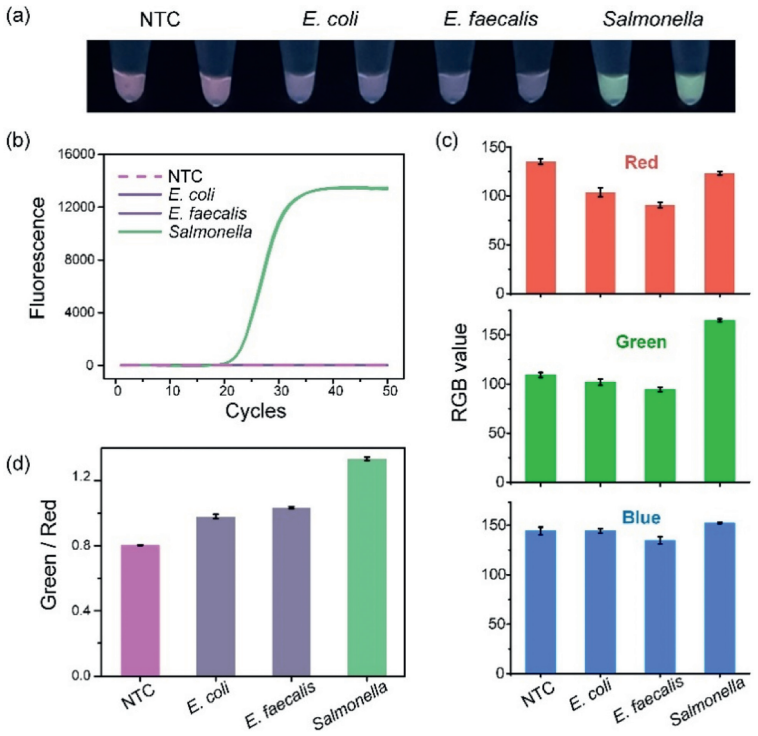

Fig. 4. Detection specificity among *Salmonella* and other bacterial pathogens. (a) Naked-eye visualization results. (b) Real-time amplification curves. (c) RGB values of different endpoint PCR products. (d) The Green/Red ratio of different samples.

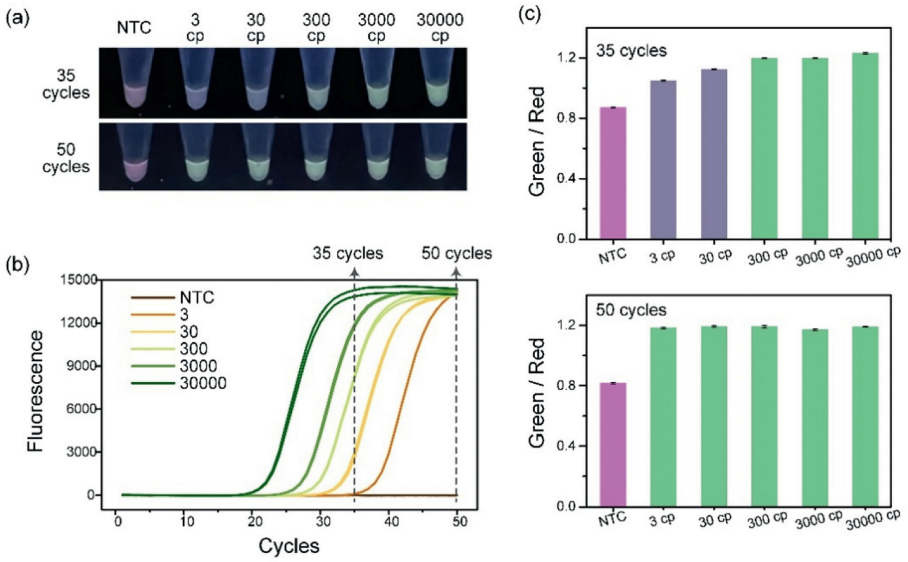

Fig. 5. Detection sensitivity of *Salmonella*. (a) Naked-eye visualization results of serially diluted samples. (b) Real-time amplification curves of serially diluted samples. (c) The Green/Red ratio of serially diluted samples after 35 cycles and 50 cycles of PCR amplification, respectively.

little as 3 copies of initial templates, indicating a limit of detection down to a single-copy level. With only 35 cycles of amplification, the 3-cp and 30-cp samples still presented negative outcomes with a lavender color while the 300-cp sample was positive with an obvious green color. For real-time PCR as shown in Fig. 5b, after 35 cycles of amplification, the result of the 3-cp sample was negative while the outcome of the 30-cp sample was suspicious and that of the 300-cp sample was positive. The sensitivity of the naked-eye detection approach is comparable with real-time PCR.

We further performed RGB analysis of the serially diluted samples (Fig. S5 in Supporting information) and measured the G/R ratio after 35 cycles and 50 cycles of PCR amplification, respectively. As shown in Fig. 5c, after 30 PCR cycles, the G/R ratio gradually increased from 3-cp samples to 30,000-cp samples, which showed a similar tendency with the fluorescence as recorded *via* the real-time PCR cycler. After 50 PCR cycles, the G/R ratio of all positive samples, as well as their fluorescence, reached the plateau. By comparing the G/R ratio shown in Fig. 5c and the real-time amplification curves in Fig. 5b, it could be concluded that the G/R ratio well characterized the amplification process, further proving it to be a good indicator for the color of PCR products.

With the proposed sensing scheme, the endpoint PCR products would display three color patterns, with a red color indicating no DNA template, a green color representing successful amplification

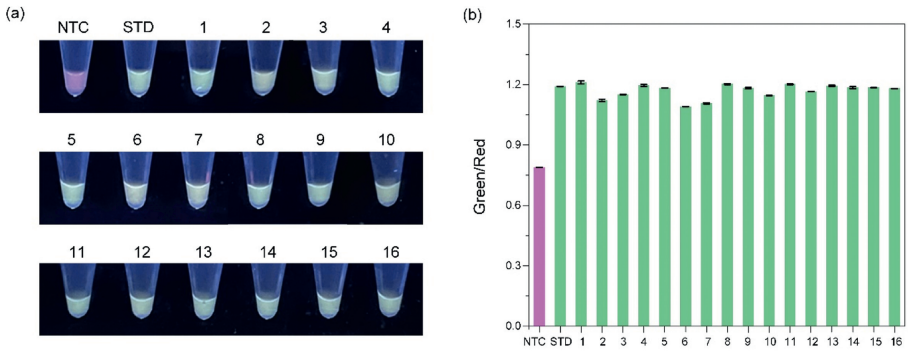

Fig. 6. Detection results of real samples with the proposed sensing strategy. (a) Visual images of the real samples *via* the naked eye. (b) G/R ratios of visual images of real samples. "STD" stands for the *Salmonella enterica* strain ATCC 14028, which was used as a positive control here.

of specific templates, and a lavender color indicating the existence of nonspecific templates or an insufficient amplification of specific templates. To keep things simple, we suggest running full cycles of PCR (50 cycles) in real-world applications, so that the lavender color would serve as a sign of negative results while the red color would imply missing templates, which might stem from failures in DNA extraction or other maloperations.

The above results demonstrated that the proposed ratiometric fluorescence sensing strategy could sensitively and selectively detect *Salmonella* DNA. To further evaluate the system's applicability with real *Salmonella* samples, we tested with 16 samples that were obtained from the Zhuhai Center for Disease Control and Prevention, where the samples were identified to be *Salmone*lla *enterica* with standard culture-based methods and serological tests. Detailed information on the samples is shown in Table S2 (Supporting information). As shown in Fig. 6a, despite their different serological properties, the 16 samples were all determined to be positive with the proposed sensing strategy. As shown in Fig. 6b, the G/R ratios among these samples varied slightly, but all stood out from the NTC. The testing results from the ratiometric fluorescence detection strategy were 100% consistent with standard culture-based methods and validated the efficacy and applicability of the proposed system.

In conclusion, based on the ratiometric fluorescence signals from SG and HNB, we hereby established a naked-eye sensing system to detect PCR-amplified DNA in a snapshot. The combination of the two dyes was fully exploited to enhance the green fluorescence from SG to the greatest extent while HNB's red fluorescence remained unchanged and served as a background. The detection approach required minimal modifications of conventional PCR assays and achieved one-pot detection of PCR results under UV excitation. Reaction time and cost of detection were reduced to the greatest extent without sacrificing detection performance. In detecting *Salmonella*, we characterized the detection approach with single-copy sensitivity, high specificity, and significant robustness as indicated by the broad dynamic range of effective dye combinations. Further, a simple RGB analysis of the visualized images with a color-picking smartphone app provided users with numerical indicators of the endpoint products and formed a supplement to the intuitive naked-eye visualization result. When combined with portable thermal cyclers [38,39], the proposed sensing scheme would serve as a system solution for field use of the vast majority of PCR-based applications, especially in resource-limited settings.

Declaration of competing interest

The authors declare that they have no known competing financial interests or personal relationships that could have appeared to influence the work reported in this paper.

CRediT authorship contribution statement

Ren Shen: Writing – original draft, Validation, Methodology, Investigation, Conceptualization. **Yanmei Fang:** Writing – review & editing, Supervision, Funding acquisition. **Chunxiao Yang:** Resources. **Quande Wei:** Resources. **Pui-In Mak:** Supervision, Funding acquisition. **Rui P. Martins:** Supervision. **Yanwei Jia:** Resources, Methodology.

Acknowledgments

This work was supported by the Macao Science and Technology Development Fund (FDCT) (Nos. FDCT 0029/2021/A1, FDCT0002/2021/AKP, 004/2023/SKL, 0036/2021/APD); University of Macau (No. MYRG-GRG2023–00034-IME, SRG2024-00057-IME); Dr. Stanley Ho Medical Development Foundation (No. SHMDF-OIRFS/2024/001); Zhuhai Huafa Group (No. HF-006–2021); Guangdong Science and Technology Department (No. 2022A0505030022). We also thank the technical and administrative team of the State-Key Laboratory of Analog and Mixed-Signal VLSI at the University of Macau for all their support.

Supplementary materials

Supplementary material associated with this article can be found, in the online version, at doi:10.1016/j.cclet.2024.110143.

References

[1] O. Ehuwa, A.K. Jaiswal, S. Jaiswal, Foods 10 (2021) 907.
[2] G. Xing, W. Zhang, N. Li, Q. Pu, J.M. Lin, Chin. Chem. Lett. 33 (2022) 1743–1751.
[3] W. Qi, S. Wang, L. Wang, et al., Chin. Chem. Lett. 34 (2023) 107360.
[4] M.S. Awang, Y. Bustami, H.H. Hamzah, et al., Biosensors 11 (2021) 346.
[5] X. Huo, L. Wang, W. Qi, et al., Chin. Chem. Lett. 33 (2022) 2091–2095.
[6] G. Cai, Y. Wang, Y. Zhang, L. Zheng, J. Lin, Chin. Chem. Lett. 34 (2023) 108059.
[7] J.A. Crump, M. Sjölund-Karlsson, M.A. Gordon, C.M. Parry, Clin. Microbiol. Rev. 28 (2015) 901–937.
[8] G. Xing, Y. Shang, X. Wang, et al., Chin. Chem. Lett. 35 (2024) 109491.
[9] M. Bugarel, A. Tudor, G.H. Loneragan, K.K. Nightingale, J. Microbiol. Methods 134 (2017) 14–20.
[10] S.C. Ricke, S.A. Kim, Z. Shi, S.H. Park, J. Appl. Microbiol. 125 (2018) 313–327.
[11] S. Umesha, H.M. Manukumar, Crit. Rev. Food Sci. Nutr. 58 (2018) 84–104.
[12] R.K. Saiki, D.H. Gelfand, S. Stoffel, et al., Science 239 (1988) 487–491.
[13] R. Higuchi, C. Fockler, G. Dollinger, R. Watson, BioTechnol 11 (1993) 1026–1030.
[14] D.C. Schwartz, M. Koval, Nature 338 (1989) 520–522.
[15] R. Yamashige, M. Kimoto, R. Okumura, I. Hirao, J. Am. Chem. Soc. 140 (2018) 14038–14041.
[16] P. Valentini, P.P. Pompa, Angew. Chem. Int. Ed. 55 (2016) 2157–2160.
[17] F. Li, F. Li, G. Yang, et al., Sens. Actuators B: Chem. 255 (2018) 1455–1461.
[18] T.T. Tsai, C.A. Chen, N.Y.J. Ho, S. Yang, C.F. Chen, ACS Sens. 4 (2019) 2885–2892.
[19] H.B. Wang, L.H. Ma, T. Zhang, et al., Anal. Chim. Acta 1093 (2020) 106–114.
[20] S.K. Kim, Y.H. Oh, D.H. Ko, et al., Biosensors 12 (2022) 744.
[21] K.M. Ririe, R.P. Rasmussen, C.T. Wittwer, Anal. Biochem. 245 (1997) 154–160.
[22] H. Zipper, H. Brunner, J. Bernhagen, F. Vitzthum, Nucleic Acids Res. 32 (2004) e103.

[23] M. Goto, E. Honda, A. Ogura, A. Nomoto, K.I. Hanaki, BioTechniques 46 (2009) 167–172.
[24] X. Ding, W. Wu, Q. Zhu, et al., Anal. Chem. 87 (2015) 10306–10314.
[25] Y. He, Z. Lu, K. Liu, et al., Sens. Actuators B: Chem. 399 (2024) 134851.
[26] K. Nath, J.W. Sarosy, J. Hahn, C.J.D. Como, J. Biochem. Biophys. Methods 42 (2000) 15–29.
[27] H. Gudnason, M. Dufva, D.D. Bang, A. Wolff, Nucleic Acids Res. 35 (2007) e127.
[28] J.E. Kong, Q. Wei, D. Tseng, et al., ACS Nano 11 (2017) 2934–2943.
[29] R. Shen, Y. Jia, P.I. Mak, R.P. Martins, Lab Chip 20 (2020) 1928–1938.
[30] J.W. Park, Biosensors 12 (2022) 857.
[31] Q. Yang, H. Yang, N. Yuan, et al., Food Chem. 393 (2022) 133408.
[32] J.M. Kim, H.R. Kim, J.S. Baek, et al., Pathogens 12 (2023) 921.
[33] Y. Li, H. Xue, Y. Fei, et al., Food Chem. 405 (2023) 134975.
[34] M.C.B. Prasad, A.A.P. Milton, V.K. Menon, et al., Food Control 155 (2024) 110081.
[35] M. Varona, J.L. Anderson, Anal. Chem. 91 (2019) 6991–6995.
[36] M. Sidstedt, P. Rådström, J. Hedman, Anal. Bioanal. Chem. 412 (2020) 2009–2023.
[37] W. Li, X. Zhang, X. Hu, et al., J. Hazard. Mater. 408 (2021) 124872.
[38] J. Zhang, Z. Yang, L. Liu, et al., Biosensors 13 (2023) 234.
[39] Y. Fang, Y. Wang, L. Zhu, et al., Chin. Chem. Lett. 34 (2023) 108092.